INTERNATIONAL JOURNAL OF HYDROGEN ENERGY 45 (2020) 29246–29258

Available online at www.sciencedirect.com

ScienceDirect

journal homepage: www.elsevier.com/locate/he

Air mass flow and pressure optimisation of a PEM fuel cell range extender system

Johannes Hoeflinger[*], *Peter Hofmann*

Vienna University of Technology, Getreidemarkt 9, Vienna, 1060, Austria

HIGHLIGHTS

- At high loads, the system efficiency is higher at high air pressure and low mass flow.
- At low loads, the system efficiency is higher at low air pressure and high mass flow.
- Maximum system efficiency is 55.21% at the lowest continuous load point.
- Maximum system efficiency is 43.74% at the highest continuous load point.

GRAPHICAL ABSTRACT

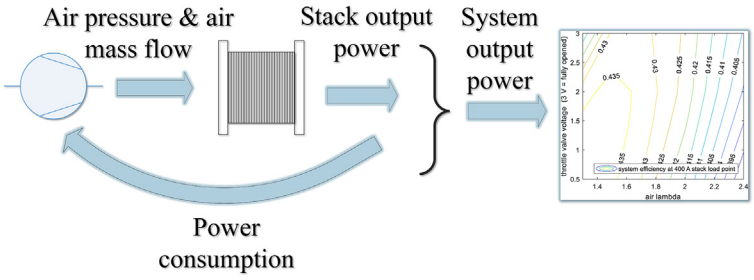

ARTICLE INFO

Article history:
Received 20 April 2020
Received in revised form
1 July 2020
Accepted 19 July 2020
Available online 14 August 2020

Keywords:
Hydrogen PEM fuel cell
Range extender
Air supply system
Fuel cell model
Fuel cell operating parameter influences
Fuel cell air compressor

ABSTRACT

In order to eliminate the local CO_2 emissions from vehicles and to combat the associated climate change, the classic internal combustion engine can be replaced by an electric motor. The two most advantageous variants for the necessary electrical energy storage in the vehicle are currently the purely electrochemical storage in batteries and the chemical storage in hydrogen with subsequent conversion into electrical energy by means of a fuel cell stack. The two variants can also be combined in a battery electric vehicle with a fuel cell range extender, so that the vehicle can be refuelled either purely electrically or using hydrogen. The air compressor, a key component of a PEM fuel cell system, can be operated at different air excess and pressure ratios, which influence the stack as well as the system efficiency. To asses the steady state behaviour of a PEM fuel cell range extender system, a system test bench utilising a commercially available 30 kW stack (96 cells, 409 cm^2 cell area) was developed. The influences of the operating parameters (air excess ratio 1.3 to 1.7, stack temperature 20 °C–60 °C, air compressor pressure ratio up to 1.67, load point 122 mA/cm^2 to 978 mA/cm^2) on the fuel cell stack voltage level (constant ambient relative humidity of 45%) and the corresponding system efficiency were measured by utilising current, voltage, mass flow, temperature and pressure sensors. A fuel cell stack model was presented, which correlates closely with the experimental data (0.861% relative error). The air supply components were modelled utilising a surface fit. Subsequently, the system efficiency of the validated model was optimised by varying the air mass flow and air pressure. It is shown that higher air pressures and lower air excess ratios increase the system

* *Corresponding author.*
E-mail address: johannes.hoeflinger@tuwien.ac.at (J. Hoeflinger).

https://doi.org/10.1016/j.ijhydene.2020.07.176

efficiency at high loads. The maximum achieved system efficiency is 55.21% at the lowest continuous load point and 43.74% at the highest continuous load point. Future work can utilise the test bench or the validated model for component design studies to further improve the system efficiency.

Introduction

Currently, two main types of local zero emission propulsion systems for vehicles are considered: battery electric vehicles and fuel cell vehicles. Battery electric vehicles use solely a li-ion battery to store the electric energy in the vehicle. Fuel cell vehicles utilise, in addition to a battery, a compressed hydrogen tank and a PEM fuel cell to generate electric energy from gaseous hydrogen [1]. Depending on the degree of hybridisation of the fuel cell vehicle, the propulsion system component sizing varies. If the fuel cell is used as the main power source, only a small battery can be used. Alternatively, a smaller sized fuel cell can be combined with larger battery.

A fuel cell stack needs several other components for its proper operation (BOP, balance of plant components). One of the most important components in this regard is the air compressor, which has the highest power consumption level compared to the other BOP components [2]. Moreover, the air supply system is crucial for the stable and efficient operation of a fuel cell system [3,4]. Firstly, it influences the humidity level (and humidity removal) of the stack [5,6]. Secondly, the oxygen in the air influences the stack voltage and therefore the efficiency of the stack. The air compressor can supply air at different air mass flows and air pressure levels to the stack. These operating parameters and the corresponding electric energy consumption of the compressor influence the stack and system efficiency. This work covers the system efficiency optimisation regarding the air supply parameters (air excess ratio and pressure ratio).

Besides the air supply system, also the hydrogen supply system plays a crucial role for the proper operation of the fuel cell system. However, the hydrogen supply system usually consumes less power compared to the air supply side, especially at higher loads. When the hydrogen gas enters the anode of the stack, an electric pressure control valve guarantees the desired pressure. For some systems, a water trap removes excess water from the anode. A purge valve is periodically opened to remove water and gas impurities from the anode chamber, which negatively affect the voltage level of the stack [7,8]. The energy consumption of these components are insignificant compared to the hydrogen recirculation pump. The pump speed can be controlled depending on the load point or can be set constant, so that the hydrogen flow over the membranes on the anode side guarantees the efficient water removal of the gas diffusion layers. The hydrogen for automotive fuel cell systems is usually not externally humidified [9]. The hydrogen recirculation pump has an electric energy consumption level in the range of the coolant pump and can be replaced by a passive venturi recirculation for advanced systems so that no electric power is consumed at all.

Generally, a higher air mass flow increases the stack voltage (and stack efficiency) [10,11]. At lower mass flows, the stable operation of the stack cannot be guaranteed due to the higher propensity of water condensation and oxygen starvation [12]. High velocity air is needed to remove the produced water at the cathode side of the stack. At high air mass flows, the oxygen partial pressure is also higher thus increasing the stack voltage. However, after longer operation at high air mass flows the membranes are not humidified enough and drying up can occur. The lambda value λ (air excess ratio) is calculated according to Eq. (1), which is the air mass flow actually flowing through the stack $\dot{m}_{air}$ divided by the air mass flow which would be needed if all oxygen is used up by the reaction inside the stack (stoichiometric air mass flow). M_{air} is the molar mass of air, x_{O_2} is the mole fraction of oxygen in air, I the stack current, n the number of cells in the stack and F is the Faraday constant. Typical values of air excess ratios are between 1.5 and 3.0, depending on the system parameters and design [13–16].

$$\lambda = \frac{\dot{m}_{air}}{\left(\frac{InM_{air}}{4Fx_{O_2}}\right)} \quad (1)$$

The pressure inside the cathode of the stack is determined by the pressure ratio of the air compressor and the pressure drop of the stack. When a throttle valve after the fuel cell stack is used, the pressure resistance and the pressure at the cathode side can be increased. If an expander (turbine) is used instead of the throttle valve, the energy of the pressurized air mass flow can be harnessed to increase the system efficiency [13,17–19]. The maximum air inlet pressure of the stack is limited by the surge line of the air compressor [20]. The lowest pressure is limited by the pressure drop of the stack and the choke line of the air compressor. Operating points below the choke line and above the surge line must be avoided to prevent damage to the compressor due to overheating issues, high pressures and pressure fluctuations [21]. The determination of the surge line can be difficult. A typical pumping sound (unstable operation) is usually observed when the pressure ratio is too high and a stall occurs above the surge line. In this case, the pressure resistance must be reduced to avoid damage to the compressor.

Higher reactant pressures result in higher fuel cell stack voltage, power and efficiency [22,23]. Generally, if the operating pressure of PEM fuel cells is increased above 4 bar, the effect of the voltage increase is getting smaller due to mass

transport issues. Therefore, the optimal PEM-fuel cell operating pressure lies typically between 3 and 4 bar [24]. Due to the limit of the maximum pressure ratio of a single turbo compressor, a second turbo compressor in series or a different type of compressor (e.g., a screw compressor) could be used to achieve higher pressures and stack voltages. In Ref. [25] positive or negative pressure net effects for the system efficiency are proposed, depending on the system parameters (compressor efficiency and pressure stack voltage influence). In Ref. [26] an optimal system efficiency operating pressure of 2 bar (using a screw compressor) is stated. [27] investigated the effect of different pressure levels and air excess ratios on the net cell voltage level (cell voltage subtracted by the parasitic losses for the compression of the air) by the utilising the Nernst equation. The optimum point was found the be at 2 bar for an air excess ratio of 2. For air excess ratios greater than 3, the net voltage level was found to be negative. [28] analysed a 80 kW fuel cell vehicle with regard to the air blower speed and a backpressure control valve. It was found that at low loads, the system power decreases when the backpressure valve angle is increased (opened up) and the influence of the blower speed is higher when the valve is at higher angles (higher system power at lower blower speeds). At high loads, for most blower speeds, the system power increases when the backpressure valve is opened up and reaches a maximum after decreasing again if the valve is further opened up. This behaviour may be attributed to the modelled humidity inside the stack, which is influenced by both the blower speed (air excess ratio) and backpressure level.

This paper evaluates the optimal system efficiency of a PEM fuel cell system with a turbo compressor at different steady state load points. The novelty of this work is the verified model development and combined investigation of the air pressure and air mass flow on the system efficiency of a 25 kW system. The trade-off between higher oxygen partial pressure inside the stack (higher efficiency) and additional power consumption of the turbo air compressor (lower efficiency) was analysed in detail for 4 different load points. For this purpose, a 0-dimensional fuel cell stack model was developed, which is sensitive to three input variables (load current, temperature and oxygen partial pressure). For the cathode of the fuel cell stack, a 1-dimensional modelling approach was used. Based on this 1-dimensional approach, a 0-dimensional average oxygen partial pressure value was calculated which was utilized as input for the stack model. The oxygen partial pressure depends on the air excess ratio, the compressor pressure ratio and the pressure drop of the stack. As a result, the developed models are sensitive to air mass flow and air pressure and were used to asses the system efficiency with regard to these variables. Furthermore, all the used models were verified my measured data to obtain reliable simulation results.

Methodology

For the investigations of this work, experimental and theoretical methods were used. Firstly, the set up and the components of the fuel cell system test bench are outlined. Secondly, the modelling methodology and the used equations for the theoretical investigations are described.

Experimental set up

In order to obtain the experimental data, a PEM fuel cell system test bench was developed. The main components are a 30 kW PEM fuel cell stack, a turbo air compressor to supply ambient air to the cathode side of the stack, a hydrogen recirculation pump on the anode side and a coolant pump for the stack waste heat removal. Taking all these components into account results in a maximum electric system power of 25 kW. Fig. 1 depicts the test bench set up.

The load of the stack is controlled by a battery simulator, either the voltage level or the load current of the stack can be set. The electric energy generated by the stack is fed into the electric grid. Fig. 2 shows an overview of the used test bench components. The reaction air path of the test bench includes an activated carbon air filter, an air compressor, an intercooler, the cathode side of the stack and an electrically controlled throttle valve after the stack. The air filter counteracts cell voltage degradation and possible damage to the electrode membrane assembly by reducing air feed impurities

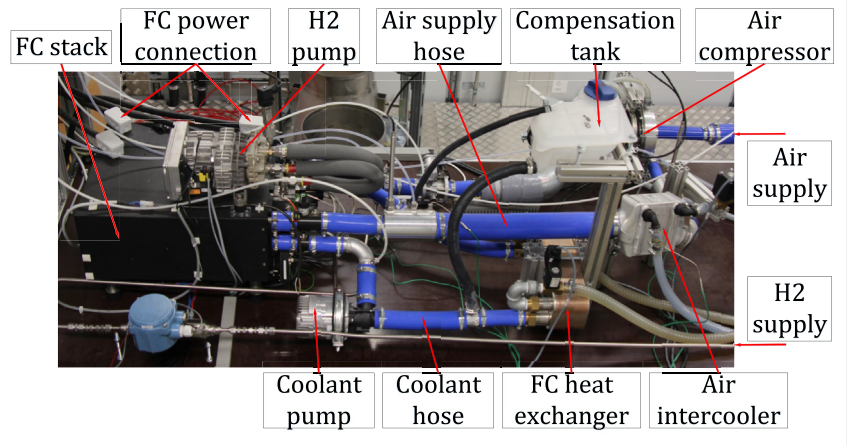

Fig. 1 – Fuel cell test bench.

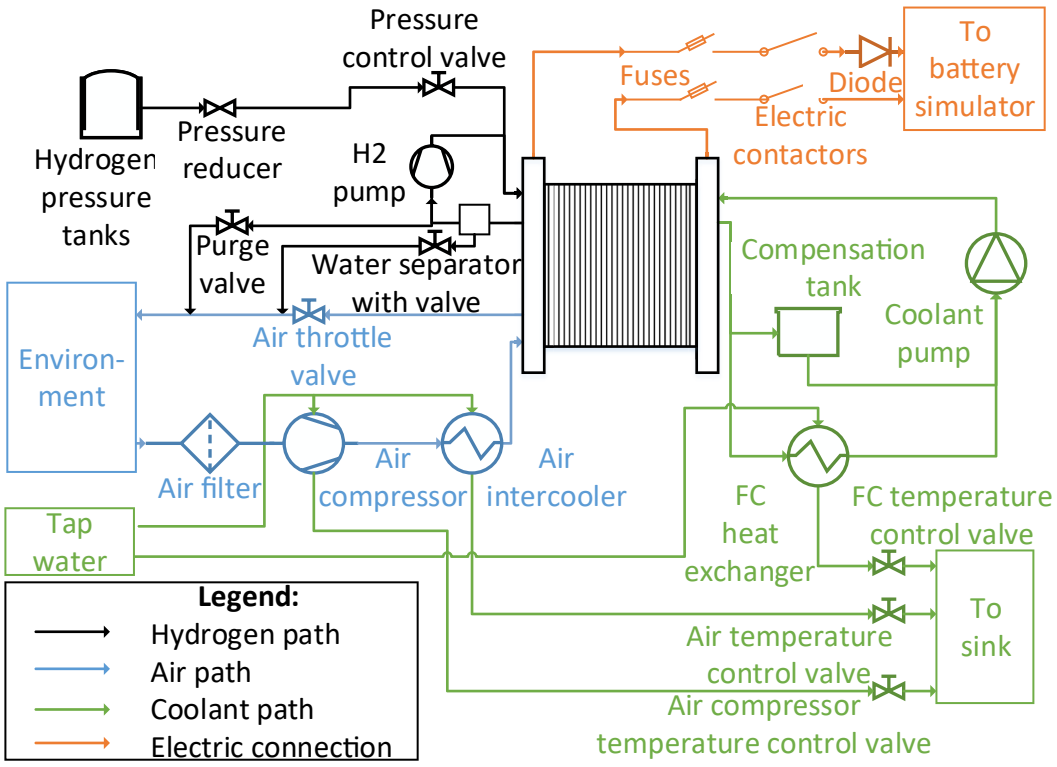

Fig. 2 – Schematic diagram of the fuel cell test bench.

[29]. With the throttle valve, the back pressure can be varied to assess different air pressure levels. The hydrogen path includes an electrically controlled pressure reducer, which is used to set the anode pressure level. The hydrogen is pumped by the hydrogen recirculation pump through the anode side of the stack. A purge valve and a water trap remove excess water from the anode, which, along with other gas impurities, impairs the performance of the stack [7,8]. The coolant circuit of the stack is thermally connected by a plate heat exchanger to the tap water side. The temperature level of the stack is controlled by a flow control valve on the tap water side. Likewise, the air compressor and the intercooler are cooled by tap water. Pressure, temperature, mass flow, relative humidity, electric current and voltage sensors are integrated into the test bench for a detailed analysis. The control software of the test bench was specifically designed for the independent and arbitrary control of all operating parameters.

Modelling

The experimental data was used to develop a fuel cell system model. Firstly, different model equations of the polarisation curve were utilized to replicate the measured behaviour of the stack in steady state operation. Secondly, a surface fit was fitted to the measured data for the steady state modelling of the air supply components. As a result, a verified model which describes the measured parameter influences was developed.

Stack model

The voltage-current relation of a fuel cell stack can be modelled by the polarisation curve V, Eq. (2) [25],

$$V = E_{OC} - V_{act} - V_{ohm} - V_{conc} \quad (2)$$

where E_{OC} is the open circuit voltage, V_{act} are the activation voltage losses, V_{ohm} are the ohmic voltage losses and V_{conc} are the concentration voltage losses. At low loads, the activation losses predominate, the ohmic losses result in a linear voltage loss across all load levels and the concentration losses increase at high loads. The three voltage losses can be modelled electric current and temperature dependent, Eqs. (3-6) [25,30,31],

Table 1 – Constant operating parameters and standard values of the fuel cell system.

Operating parameter	Value
Continuous fuel cell current	120–400 A
Air compressor pressure ratio at 400 A	1.35 (open throttle valve)
Anode pressure	700 mbar
Stack coolant inlet temperature	55°C
H2 pump speed	4000 RPM
Air excess ratio (air lambda)	1.5
Ambient temperature	20°C
Relative humidity of ambient air	45%

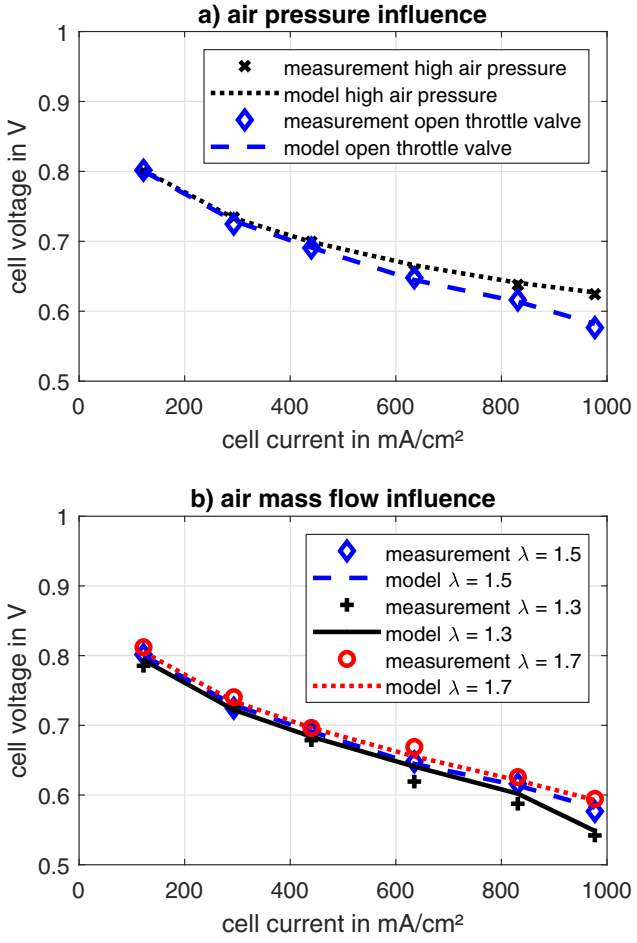

Fig. 3 – Measured and modelled air supply influence on the polarisation curve [34].

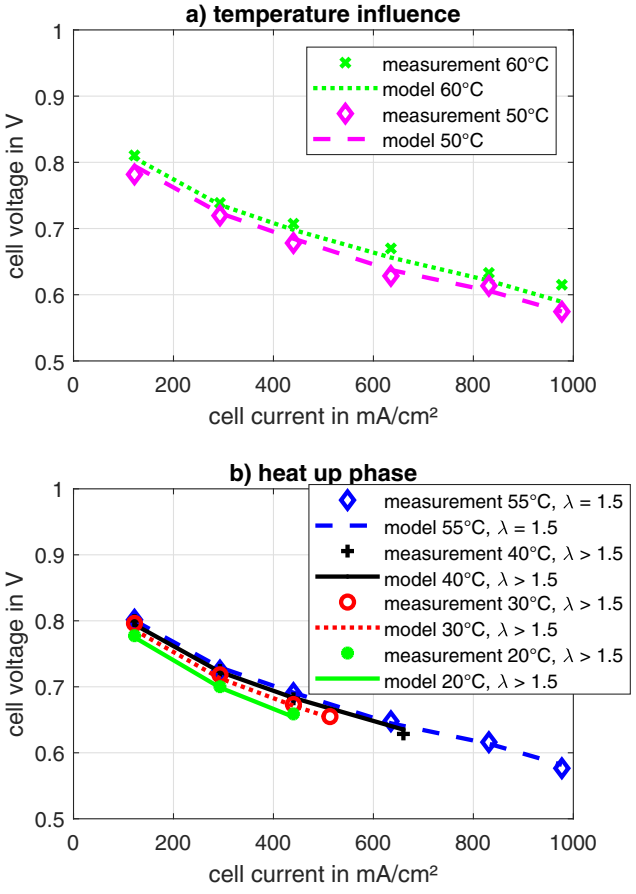

Fig. 4 – Measured and modelled temperature influence on the polarisation curve [34].

$$\Delta V_{act} = AT \ln\left(\frac{i + i_n}{i_0}\right) \tag{3}$$

$$\Delta V_{ohm} = i r_{ohm} \tag{4}$$

$$r_{ohm} = M \exp\left(\frac{N}{T}\right) \tag{5}$$

$$\Delta V_{conc} = BT \ln\left(\frac{i_{limit}}{i_{limit} - i}\right) \tag{6}$$

where T is the stack temperature, i is the load current density, $i_n = 2$ mA the internal current density, i_0 is the exchange current density, r_{ohm} is ohmic resistance per cell area (specific ohmic resistance), i_{limit} is the limiting current density, A, B, M and N are model constants.

If the influence of the air supply system is taken into account, the oxygen partial pressure must be considered as well. Subsequently, the oxygen partial pressure p_{O_2} and the temperature T were integrated into the equations of the open circuit voltage E_{OC} [32], the exchange current density i_0 [33] and the limiting current density i_{limit} [30,31], Eqs. (7)–(9) [34].

$$E_{OC} = 1.229 - 8.5 \cdot 10^{-4} \cdot (T - T_{ref}) + 4.3085 \cdot 10^{-5} \cdot T \cdot 0.5 \cdot \ln\left(p_{O_2}\right) \tag{7}$$

$$i_0 = D\left(\frac{p_{O_2}}{p_{ref}}\right)^{\gamma} \exp\left(-\frac{Z}{T}\left(1 - \frac{T}{T_{ref}}\right)\right) \tag{8}$$

$$i_{limit} = C\frac{p_{O_2}}{T} \tag{9}$$

T_{ref} is the reference temperature (298.15 K), p_{ref} is the reference pressure (0.21 bar), and C, D, γ and Z are model constants.

Table 2 – Model parameters obtained by parameter fitting.

Parameter	Value	Unit	Voltage loss
A	0,0002045	V/K	Activation losses
B	4,308E-05	V/K	Concentration losses
C	222	AK/N	Concentration losses
D	0,15158	mA/cm²	Activation losses
Γ	1,1085	–	Activation losses
M	2,01E-07	kΩcm²	Ohmic losses
N	1924,99	K	Ohmic losses
Z	4903,81	K	Activation losses

Table 3 – Relative error of the model.

Operating condition	relative error *e* in %
Standard	0.4083
High air pressure	0.407
60°C	1.595
50°C	1.02
40°C	0.864
30°C	0.677
20°C	0.418
Lambda 1.7	1.267
Lambda 1.3	0.737
Overall error	0.861

These equations describe the influence of the temperature and oxygen partial pressure on the voltage level of the stack.

In general, a higher oxygen partial pressure increases the voltage level. The oxygen partial pressure can either be increased by a higher overall air pressure level or by a higher air mass flow. However, a higher air pressure level and higher air mass flow also result in higher electric energy consumption of the air compressor. The optimum point in dependence of these two variables at different fuel cell stack load points calculated by the model are presented in the results section. For the model calculations, a linear pressure drop along the gas channels of the stack is assumed, if a more detailed analysis is needed, 3-D CFD calculations can by applied [35]. Other operating parameters such as the hydrogen pressure or the hydrogen air mass flow showed no effect on the measured stack voltage level within the possible value ranges and were therefore not included in the model. Table 1 depicts the standard operating conditions of the fuel cell system.

The correlation of the model data and the measured values of the air supply parameter variation can be seen in Fig. 3. The stack voltage was divided by the number of cells (96) and the stack current was divided by the active cell area (409 cm^2) to obtain comparable data on the cell level. Computational Fluid Dynamics (CFD) simulation results of [36] show that at low loads, the pressure has hardly any influence on the cell voltage level. However, at 1000 mA/cm^2, the influence is

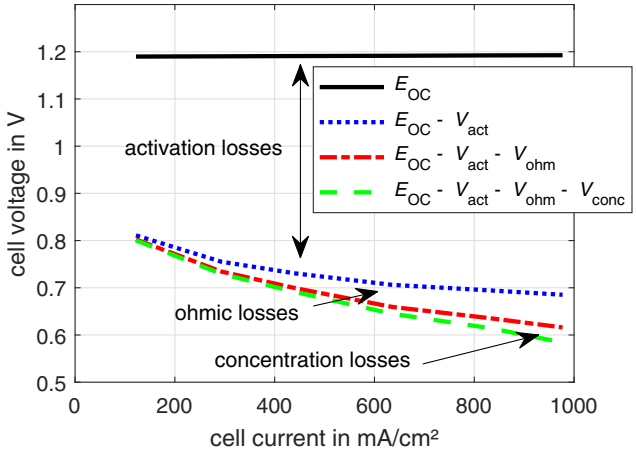

Fig. 5 – Influences of the voltage losses on the polarisation curve at standard operating conditions according to Table 1.

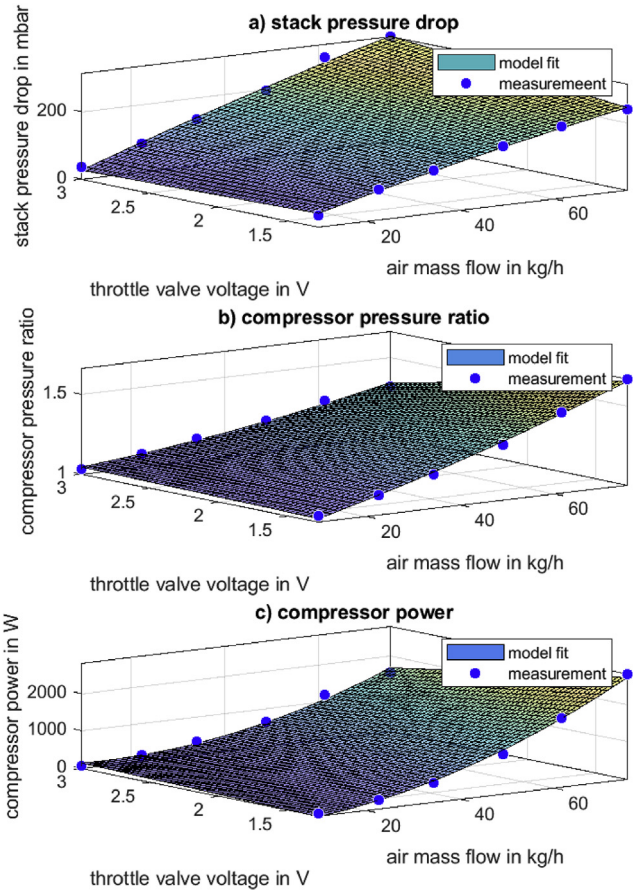

Fig. 6 – Measured and modelled stack pressure drop a), compressor pressure ratio b) and compressor power c).

0.075 V/bar at an air stoichiometry of 2. This value is about half of the value of 0.147 V/bar at an air stoichiometry of 1.5 found by the measurements in this work. The actual value of the air supply system which influences the different voltage levels of the fuel cell is the oxygen partial pressure. With higher air mass flow, the oxygen partial pressure increases inside the cathode of the stack. These oxygen partial pressure values result in the different voltage levels of the mathematical model. The influence on the voltage level is slightly higher at lower stoichiometry (1.3 and 1.5 compared to 1.5 and 1.7), which is similar to the results found in Ref. [37]. Not only a higher air mass flow results in higher oxygen partial pressure but also a higher overall pressure level. For the operation with the throttled air valve position, the voltage of the measured data and the mathematical model increase in the right amount. The temperature effect of the measured data and the model can be seen in Fig. 4a).

The combined effect of temperature and oxygen partial pressure variation of the model and the measured data are depicted in Fig. 4b) during the heat up process. During heat up, a higher air mass flow counteracts the higher water condensation propensity. The two contradicting effects (voltage increase of higher mass flow and voltage decrease of lower temperature) are described by the model.

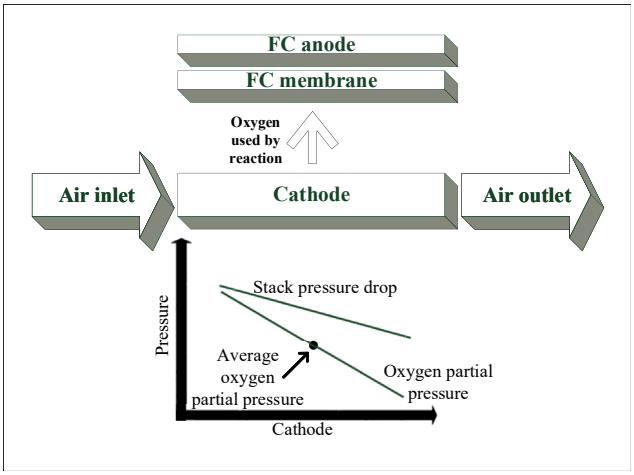

Fig. 7 – Schematic overview of the oxygen partial pressure drop inside the fuel cell stack [34].

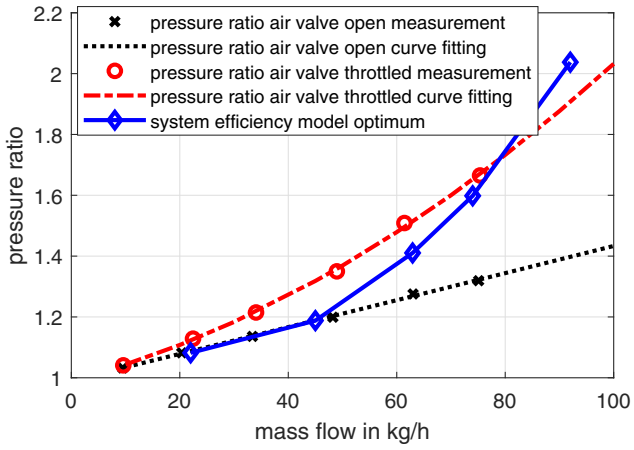

Fig. 8 – Optimal system efficiency air compressor operation at an air excess ratio of 1.5.

The constant parameter values in Table 2 were obtained for the model by parameter fitting to the measured data. Hence, a model was developed which is sensitive to the load current, the temperature and the oxygen partial pressure. Depending on the actual operating conditions, the model describes the measured influences.

The accuracy of the model is quantified by the relative error e between the model voltage V_{model} and the measured data points V_{meas}, Eq. (10).

$$e = \left| \frac{V_{meas} - V_{model}}{V_{meas}} \right| \tag{10}$$

For all nine measured polarisation curves the average relative error is depicted in Table 3. The overall relative error is 0.861% and the largest model error of 1.595% was obtained for the polarisation curve at 60 °C (which also contains the largest error of a single data point of 3.761% at 0.98 A/cm^2).

Fig. 5 shows the modelled effect of the three different voltage losses on the polarisation curve at standard operating conditions. As can be seen, the activation losses account for the largest voltage loss. The ohmic and concentration losses are comparably small and increase with higher cell load.

Compressor and stack pressure drop modelling

To investigate the influences of the air supply system on the system efficiency, a surface fit was used for the air compressor and stack pressure drop modelling, Eq. (11).

$$f(\dot{m}, V_{throttle}) = p_{00} + p_{10}\dot{m} + p_{01}V_{throttle} + p_{20}\dot{m}^2 + p_{11}\dot{m}V_{throttle} \tag{11}$$

$\dot{m}$ is the air mass flow and $V_{throttle}$ the air throttle valve voltage.

The pressure drop of the stack $p_{drop,stack}(\dot{m}, V_{throttle})$, the compressor pressure ratio $\pi(\dot{m}, V_{throttle})$ and the compressor power consumption $\dot{W}_{compr}(\dot{m}, V_{throttle})$ were modelled depending on these two parameters. Hence, not only the measured data points were analysed but also values between the measured points and points outside of the measurement range (through extrapolation). This is important in order to obtain information about operating conditions which could not be measured with the current system configuration (e.g., compressor pressure ratios above the surge line) or various combinations of different operating conditions (pressure ratio and air mass flow) which require a comparably high amount of effort and time at the fuel cell test bench. This information provides indications for further system development steps.

Fig. 6 shows the surface fits of the stack pressure drop a), compressor pressure ratio b) and compressor power c) depending on the air mass flow and the throttle valve voltage level. Lower throttle valve voltages increase the pressure resistance (closing throttle valve) and, therefore, the pressure drop. Accordingly, the density of the air increases at higher pressures and the flow velocity decreases, so that the actual pressure drop over the stack is lower. Higher air mass flows increase the pressure drop due to the higher flow velocities. In the same manner, the pressure ratio surface fit of the air compressor was obtained. Higher air mass flows and a lower throttle valve voltage (higher flow resistance) increase the pressure ratio. Similar tendencies of the pressure ratio can be observed for the compressor power consumption. Higher air mass flows and higher pressures increase the electric power demand of the electric machine of the compressor.

Table 4 – Coefficients of the air compressor and stack pressure drop model.

Coefficient	p_{00}	p_{10}	p_{01}	p_{20}	p_{11}
Stack pressure drop $p_{drop,stack}$	27.49	2.832	−16.2	−0.007953	0.7361
Compressor pressure ratio π	0.9048	0.01079	0.03926	2.917e-05	−0.002919
Compressor power consumption $\dot{W}_{compr}$	−341.2	18.98	184	0.4232	−10.38

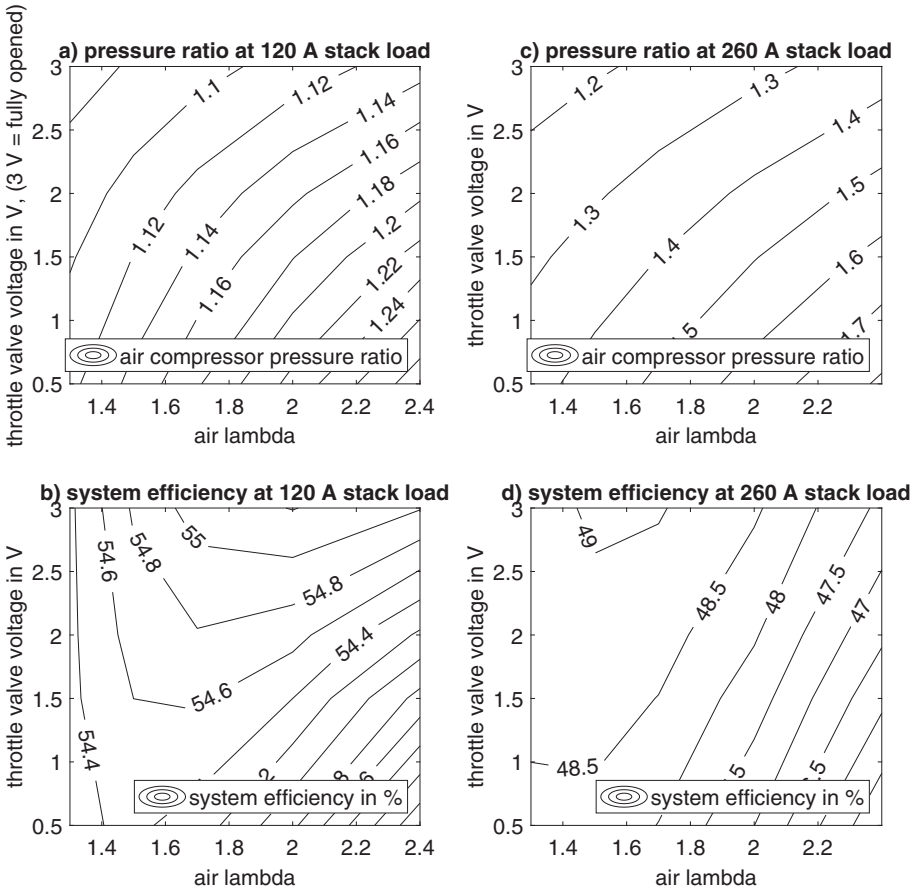

Fig. 9 – Pressure ratio of the air compressor and fuel cell system efficiency at 120 A and 260 A stack load point.

Depending on the air mass flow (air excess ratio) and the throttle valve position (resulting compressor pressure ratio), and the stack pressure drop, the average oxygen partial pressure at the cathode side of the stack is calculated. Fig. 7 shows schematically the assumed 1-dimensional pressure loss of the stack cathode. The stack flow field (parallel, serpentine, etc.) of the bipolar plates (the plates typically consist of graphite, aluminium, stainless steel or titanium with surface modifications [38–41]) influences the pressure and mass flow distribution inside the stack. However, for simplicity reasons and the general applicability of the method, the specific characteristics of the flow field were not considered but the inlet and outlet pressure of the stack was used to calculate a 1-dimensional pressure loss across the whole stack. From the 1-dimensional pressure loss across the stack, the average oxygen partial pressure inside the stack is used for the model equations.

Eq. (12) shows the calculation of the average oxygen partial pressure inside the stack, which depends on the pressure ratio π, the stack pressure drop $p_{\mathrm{drop,stack}}$ and the air excess ratio λ (the pressure drop of the intercooler is in the range of the measurement uncertainty and can therefore be neglected). To obtain the average pressure inside the cathode of the stack, the pressure ratio of the compressor (stack inlet air pressure) is reduced by half the pressure drop of the stack. This pressure is multiplied by the oxygen fraction of air. Subsequently, the average oxygen partial pressure is reduced by the oxygen reaction rate inside the stack. The oxygen leaving the stack depends on the air excess ratio, at $\lambda = 1.5$ one third, and at $\lambda = 2$ half of the oxygen of the cathode leaves the stack unused.

$$p_{O_2} = 0.21\left(\pi - \frac{p_{\mathrm{drop,stack}}}{2}\right)\frac{\left(1+\frac{\lambda-1}{\lambda}\right)}{2} \tag{12}$$

The oxygen partial pressure was used to fit the model parameters and is taken as an input for the fuel cell model to calculate the voltage level. With this information, the efficiency of the stack and the whole system can be calculated by the verified models. For all three surface fits, a coefficient of determination of $R^2 = 0.99$ was obtained. Table 4 shows the coefficients of the three surface fits.

Results and discussion

With the developed fuel cell stack and air supply components model, calculations with regard to the whole system efficiency can be made. The stack efficiency is obtained by the ratio of the actual stack voltage V_{act} during operation and the theoretical open circuit voltage (1.25 V for a single cell) multiplied by the number of single cells in the stack $n = 96$ Eq. (13).

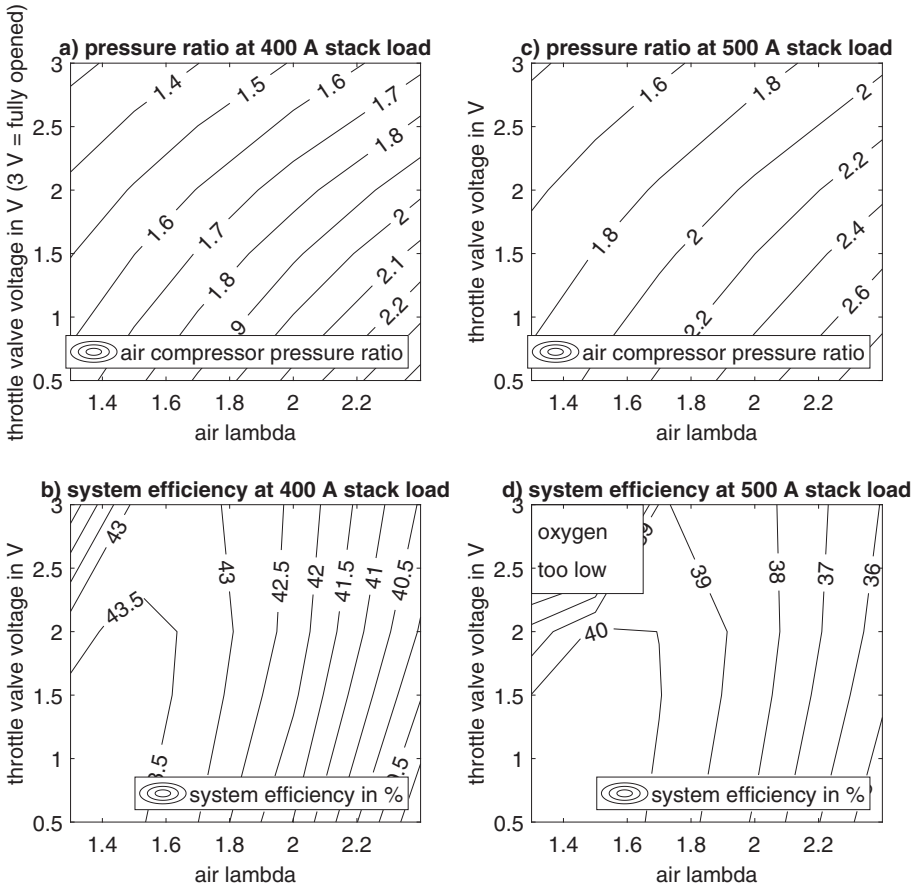

Fig. 10 – Pressure ratio of the air compressor and fuel cell system efficiency at 400 A and 500 A stack load point.

$$\eta_{stack} = \frac{V_{act}}{1.25n} \tag{13}$$

However, the fuel cell stack also needs the system components for the proper operation. To calculate the whole system efficiency η_{sys}, Eq. (14) can be used.

$$\eta_{sys} = \frac{V_{act} I - \dot{W}_{compr} - \dot{W}_{cool,pump} - \dot{W}_{hydro,pump}}{1.25In} \tag{14}$$

The stack efficiency is decreased by the electric energy consumption of the balance of plant components: the air compressor $\dot{W}_{compr}$, the constant hydrogen recirculation pump power $\dot{W}_{hydro,pump}$ (240 W) and the constant coolant pump power $\dot{W}_{cool,pump}$ (192 W).

One of the main advantages of the verified model is the comparably easy possibility to investigate different operating conditions. Especially the air mass flow and air pressure influence offer various possibilities that would need much more effort to investigate experimentally. Furthermore, the model can be used to extrapolate the operating range and give an indication of the behaviour (with regard to pressure ratio, air mass flow and temperature) after a potential hardware redesign.

The effect of the operating pressure on the cell level was investigated in Ref. [42–44]. However, not only the effects on a single cell must be taken into account but the whole system. As a result, the efficiency of the system can be optimised by finding the optimal cathode pressure. Fig. 8 shows the optimal pressure level of the air compressor with regard to system efficiency at an air excess ratio of 1.5. At low loads, the operation at low pressure is beneficial. At higher loads, the optimal pressure ratio increases. At the highest mass flow point of 92 kg/h, the model predicts an optimum above the actual possible pressure ratio of the air compressor (above the surge line). This fact suggests that for the further development of the system, higher pressure ratios of the air compressor are needed. Hence, a redesign of the air compressor (compressor wheel, operating speed, etc.) can improve the system efficiency.

However, besides the air pressure level also the air lambda value (air excess ratio) influence the system efficiency. Basically, both can be adjusted arbitrarily as long as the proper humidity management of the stack is guaranteed. Likewise, both operating variables generate higher stack voltages and efficiencies if they are increased (at the cost of higher electric power consumption of the air compressor). Hence, depending on these values the optimum point for the highest system efficiency can be calculated (the increased electric power consumption is compensated by the increased stack efficiency). The mathematical model was used to investigate four different load points of the stack:

- 120 A (lowest continuous load point)

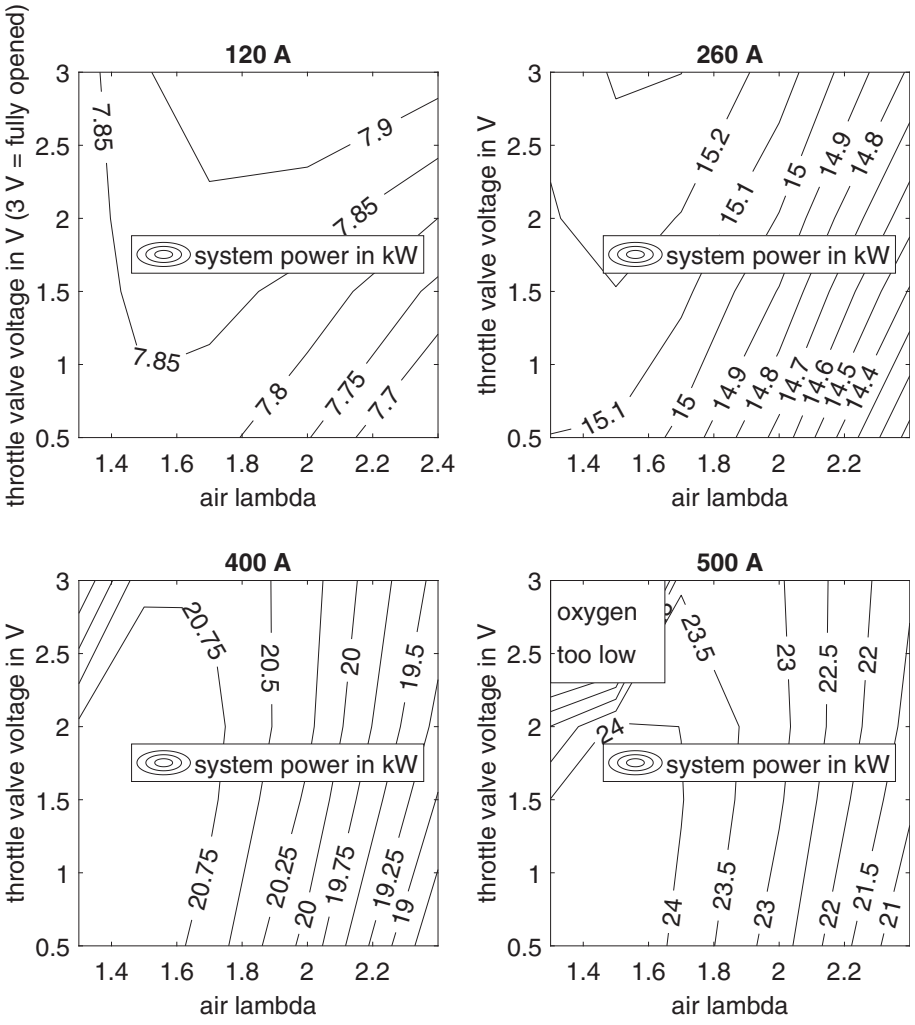

Fig. 11 – System power at four different fuel cell stack load points.

- 260 A (medium load point)
- 400 A (highest continuous load point)
- 500 A (maximum load point)

Fig. 9a) shows the pressure ratio of the air compressor and b) the fuel cell system efficiency at a stack load point of 120 A. The throttle valve voltage on the y-Axis indicates the pressure resistance after the stack. At 3 V, the throttle valve is completely open, i.e. the valve generates no pressure resistance. At 1.27 V, the throttle valve is throttled as far as possible so that the compressor operates close to the surge line. Values below 1.27 V are calculated (extrapolated) by the model to provide information which could not be measured at the test bench (operation above the surge line can cause damage to the air compressor), but could be experimentally obtained after a compressor wheel redesign. As can be seen, the pressure ratio of the compressor rises with lower throttle valve voltages (higher flow resistance) and higher air mass flows. The system efficiency was calculated for the same throttle valve voltages and air mass flows as the pressure ratio. At the load point of 120 A, the maximum system efficiency is obtained at a fully opened throttle valve and an air lambda value of 2. What is more, for a wide range of these operating conditions, the system efficiency only changes slightly (<1% in absolute terms, with the exception on the lower right).

Fig. 9c) depicts the pressure ratio and d) the fuel cell system efficiency at 260 A stack load point. The optimum system efficiency is obtained at the fully opened throttle valve position and an air lambda value of 1.5. Note that the system efficiency changes only slightly again for other conditions.

Fig. 10a) and b) shows the results for the 400 A load point. This time, the optimum is obtained at a higher pressure ratio and at an air lambda value of 1.5. The efficiency is lower if higher air mass flows are used. At very high pressure ratios, the best efficiency values are obtained at very low air lambda values.

Fig. 10c) and d) depicts the results for the maximum load point of 500 A. These calculations are an extrapolation of the model (the experimental results were recorded up to the maximum continuous load point of 400 A). In the upper left corner, the values for the system efficiency are omitted because the calculated oxygen partial pressure is not high enough to sustain this load, i.e., the stack power would be limited if no throttle valve was used and the air mass flow was not increased to higher values. The optimum system efficiency is obtained at an air lambda value of 1.3 and the highest

pressure ratio, which indicates that not only the system power but also the system efficiency can be improved at high loads by increasing the compressor pressure ratio.

Fig. 11 shows the system power of the four load points. The shape of the contour maps and the point of the maximum power are equal to those of the system efficiency. This is due to the fact that at a fixed load point of the stack in ampere, only the stack voltage level (which is proportional to the efficiency) changes with different operating conditions.

[45] investigated the air flow influence on the system efficiency. It was found that at low loads, the system efficiency is maximised at the lower bound of the air flow rate. At high loads, the system efficiency is maximised by utilising an air flow rate close to the upper bound, indicated that high air stoichiometry increases the system efficiency. Similarly [46], found that the simulated optimal air stoichiometry increases with higher load. These findings are contrary to the results found for the investigated system in this work (optimal air stoichiometry decreases with higher load) and can be attributed to different component designs and model assumptions. Furthermore, the system efficiency change in Ref. [45] amounts to 1.8% at low loads and 0.8% at high loads within the investigated air flow rate boundaries. For the investigated air excess ratios (1.3–2.4) and the air pressure levels in this work, the system efficiency changes up to 2% (lowest load point of 120 A). At the maximum load point (500 A), the change in system efficiency is higher (5%).

[47] also analysed the oxygen excess ratio and showed that the optimal system net power output can be achieved when the excess ratio is decreased (from 2.5 to 2.0) with increasing load. Similarly [48], states that the optimal oxygen excess ratio is around 3 for low loads and decreases to 2 for high loads. This trend was also found in this work, however, the optimal air excess ratios are between 2 and 1.3. [49] analysed the air excess ratio effect on the system net power while taking also the humidification into account. The optimal air excess ratio for all humidity levels at a medium load point ranges between 2.4 and 2.7. However, the investigated humidity effect is greater than the air excess ratio effect and results in higher power with higher humidification. In the current work the authors did now use the humidity as a direct input variable in the models, but the different humidity conditions are reflected by the measured voltage level of the stack.

[50] found that high pressure and high temperature improve the performance of the cell under the investigated conditions, these results are also in accordance with this work. [51] studied the optimal pressure of a 20 kW PEM fuel cell system. It was found that the operation under low pressure (atmospheric pressure at fuel cell stack air outlet) is optimal due to the inefficient compressor. However, if the compressor efficiency is increased, also the optimal pressure is increased (the additional stack efficiency gains are higher than the additional compressor power consumption). In comparison, the air pressure variation in this work showed that at low loads, the system efficiency is higher at low pressure (atmospheric pressure at fuel cell stack air outlet). At high loads the efficiency is higher at higher pressure, which indicates an advantageous efficiency for the investigated compressor at high pressure ratio and mass flow.

Conclusion

In this work, a PEM fuel cell range extender system was analysed. A test bench of a 25 kW fuel cell system was developed and the operation with all possible steady state parameter influences with regard to the efficiency was investigated. Based on the experimental data, a fuel cell stack and air supply component model was formulated. The parameters of the model equations were fitted to the measured steady state behaviour of the system. Four different operating conditions were used to fit the polarisation curve to the measured data to achieve a relative model error of 0.861%: air excess ratio variation (1.3–1.7), air pressure variation (open and throttled air valve), temperature variation (50 °C–60 °C) and the heat-up process (20 °C–40 °C at an increased air excess ratio). Furthermore, surface fits were used to model the power consumption and pressure ratio of the air turbo compressor as well as the pressure drop of the stack ($R^2 = 0.99$). The air supply system was optimised at four stack load points (120 A, 260 A, 400 A, 500 A) with regard to system efficiency by utilising the validated models. It was shown that at low loads, the efficiency is higher at low pressure levels (open throttle valve) and higher air excess ratios. At higher loads, the system behaves the other way, i.e. the efficiency is higher at high pressure values and low air excess ratios. Likewise, the maximum system power of the four load points was found to be at the same air excess ratios and pressure levels. The maximum achieved system efficiency is 55.21% at the lowest continuous load point (120 A, 7.9 kW) and 43.74% at the highest continuous load point (400 A, 20.75 kW). To further improve the system efficiency in the future, the following points represent promising adjustments: utilisation of an air humidifier, operation at increased stack temperature or operation at increased air pressure levels.

Declaration of competing interest

The authors declare that they have no known competing financial interests or personal relationships that could have appeared to influence the work reported in this paper.

Acknowledgements

Special thanks to the Austrian Ministry for Transport, Innovation and Technology (BMVIT) and the Austrian Research Promotion Agency (FFG) for financially supporting this research project in the course of the mobility of the future program.

REFERENCES

[1] Wu H-W. A review of recent development: transport and performance modeling of pem fuel cells. Appl Energy

2016;165:81–106. https://doi.org/10.1016/j.apenergy.2015.12.075. http://www.sciencedirect.com/science/article/pii/S0306261915016487.
[2] Cunningham JM, Hoffman MA, Moore RM, Friedman DJ. Requirements for a flexible and realistic air supply model for incorporation into a fuel cell vehicle (fcv) system simulation. SAE Trans 1999:3191–6.
[3] Pischinger S, Schönfelder C, Bornscheuer W, Kindl H, Wiartalla A. Integrated air supply and humidification concepts for fuel cell systems. SAE Trans 2001:86–92.
[4] Yan W-M, Wang X-D, Lee D-J, Zhang X-X, Guo Y-F, Su A. Experimental study of commercial size proton exchange membrane fuel cell performance. Appl Energy 2011;88(1):392–6. https://doi.org/10.1016/j.apenergy.2010.06.025. http://www.sciencedirect.com/science/article/pii/S0306261910002527.
[5] Pem fuel cell relative humidity (rh) and its effect on performance at high temperatures. Electrochim Acta 2008;53(16):5315–21. https://doi.org/10.1016/j.electacta.2008.02.074.
[6] Jung G-B, Lo K-F, Su A, Weng F-B, Tu C-H, Yang T-F, Chan S-H. Experimental evaluation of an ambient forced-feed air-supply pem fuel cell. Int J Hydrogen Energy 2008;vol. 33(12):2980–5. https://doi.org/10.1016/j.ijhydene.2008.03.056. 2nd World congress of young scientists on hydrogen energy systems, http://www.sciencedirect.com/science/article/pii/S0360319908003650.
[7] Kocha SS, Deliang Yang J, Yi JS. Characterization of gas crossover and its implications in pem fuel cells. AIChE J 2006;52(5):1916–25. https://doi.org/10.1002/aic.10780. https://aiche.onlinelibrary.wiley.com/doi/pdf/10.1002/aic.10780. https://aiche.onlinelibrary.wiley.com/doi/abs/10.1002/aic.10780.
[8] Rabbani A, Rokni M. Effect of nitrogen crossover on purging strategy in pem fuel cell systems. Appl Energy 2013;111:1061–70. https://doi.org/10.1016/j.apenergy.2013.06.057. http://www.sciencedirect.com/science/article/pii/S0306261913005643.
[9] Kurzweil P. Brennstoffzellentechnik. Wiesbaden: Springer Vieweg; 2003.
[10] Barbir F, Balasubramanian B, Neutzler J. Optimal operating temperature and pressure of pem fuel cell systems in automotive applications. In: Abstracts of papers of the American chemical society, vol. 218. 1155 16TH ST, NW, WASHINGTON, DC 20036 USA: Amer Chemical Soc; 1999. U637–U637.
[11] Reshetenko TV, Bender G, Bethune K, Rocheleau R. Systematic study of back pressure and anode stoichiometry effects on spatial pemfc performance distribution. Electrochim Acta 2011;56(24):8700–10. https://doi.org/10.1016/j.electacta.2011.07.058. http://www.sciencedirect.com/science/article/pii/S0013468611011029.
[12] Matraji I, Laghrouche S, Jemei S, Wack M. Robust control of the pem fuel cell air-feed system via sub-optimal second order sliding mode. Appl Energy 2013;104:945–57. https://doi.org/10.1016/j.apenergy.2012.12.012. http://www.sciencedirect.com/science/article/pii/S030626191200894X.
[13] Ji SW, Myung NS, Kim TS. Analysis of operating characteristics of a polymer electrolyte membrane fuel cell coupled with an air supply system. J Mech Sci Technol 2011;25(4):945–55. https://doi.org/10.1007/s12206-011-0138-0. URL https://doi.org/10.1007/s12206-011-0138-0.
[14] Andjar J, Segura F. Fuel cells: history and updating. a walk along two centuries. Renew Sustain Energy Rev 2009;13(9):2309–22. https://doi.org/10.1016/j.rser.2009.03.015. http://www.sciencedirect.com/science/article/pii/S1364032109001336.
[15] Kulikovsky A. The effect of stoichiometric ratio on the performance of a polymer electrolyte fuel cell. Electrochim Acta 2004;49(4):617–25. https://doi.org/10.1016/j.electacta.2003.09.016. http://www.sciencedirect.com/science/article/pii/S0013468603007321.
[16] Rabbani A, Rokni M. Dynamic characteristics of an automotive fuel cell system for transitory load changes. Sustain Energy Technol Assess 2013;1:34–43. https://doi.org/10.1016/j.seta.2012.12.003. http://www.sciencedirect.com/science/article/pii/S2213138812000057.
[17] Boettner DD, Paganelli G, Guezennec YG, Rizzoni G, Moran MJ. Proton exchange membrane fuel cell system model for automotive vehicle simulation and control. J Energy Resour Technol 2002;124(1):20–7. https://doi.org/10.1115/1.1447927. URL https://doi.org/10.1115/1.1447927. https://asmedigitalcollection.asme.org/energyresources/article-pdf/124/1/20/5887495/20＼_1.pdf.
[18] Lang O, Pischinger S, Schönfelder C, Steidten T. Compressor-expander units for mobile fuel cell systems. MTZ worldwide 2004;65(7):29–32. https://doi.org/10.1007/BF03227690. URL https://doi.org/10.1007/BF03227690.
[19] Cunningham J, Hoffman M, Eggert A, Friedman D. The implications of using an expander (turbine) in an air system of a pem fuel cell engine. In: Proceedings of the 17th international electric vehicle symposium & exposition; 2000.
[20] T. Sun, X. Zhang, B. Chen, X. Liu, Coordination control strategy for the air management of heavy vehicle fuel cell engine, Int J Hydrogen Energy:https://doi.org/10.1016/j.ijhydene.2019.10.134. URL http://www.sciencedirect.com/science/article/pii/S036031991933945X.
[21] Bao C, Ouyang M, Yi B. Modeling and optimization of the air system in polymer exchange membrane fuel cell systems. J Power Sources 2006;156(2):232–43. https://doi.org/10.1016/j.jpowsour.2005.06.008.
[22] Tafaoli-Masoule M, Shakeri M, Esmaili Q, Bahrami A. Pem fuel cell modeling and pressure investigation. Energ Source Part A 2011;33(24):2291–302. https://doi.org/10.1080/15567030903530566. doi:10.1080/15567030903530566. URL https://doi.org/10.1080/15567030903530566.
[23] Gelfi S, Stefanopoulou AG, Pukrushpan JT, Peng H. Dynamics of low-pressure and high-pressure fuel cell air supply systems. In: Proceedings of the 2003 American control conference, 2003, vol. 3. IEEE; 2003. p. 2049–54.
[24] Ahmadi N, Dadvand A, Rezazadeh S, Mirzaee I. Analysis of the operating pressure and gdl geometrical configuration effect on pem fuel cell performance. J Braz Soc Mech Sci Eng 2016;38(8):2311–25. https://doi.org/10.1007/s40430-016-0548-0. URL https://doi.org/10.1007/s40430-016-0548-0.
[25] Larminie J, Dicks A. Fuel cell systems explained. Wiley; 2003, ISBN 978-0-470-84857-9.
[26] Kim H-S, Lee D-H, Min K, Kim M. Effects of key operating parameters on the efficiency of two types of pem fuel cell systems (high-pressure and low-pressure operating) for automotive applications. J Mech Sci Technol 2005;19(4):1018–26. https://doi.org/10.1007/BF02919185. URL https://doi.org/10.1007/BF02919185.
[27] Blunier B, Miraoui A. Air management in pem fuel cells: state-of-the-art and prospectives. In: 2007 International aegean conference on electrical machines and power electronics. IEEE; 2007. p. 245–54.
[28] Kim DK, Min HE, Kong IM, Lee MK, Lee CH, Kim MS, Song HH. Parametric study on interaction of blower and back pressure control valve for a 80-kw class pem fuel cell vehicle. Int J Hydrogen Energy 2016;41(39):17595–615. https://doi.org/10.1016/j.ijhydene.2016.07.218. http://www.sciencedirect.com/science/article/pii/S0360319916322054.
[29] Shi Z, Song D, Li H, Fatih K, Tang Y, Zhang J, Wang Z, Wu S, Liu Z-S, Wang H, et al. A general model for air-side proton

exchange membrane fuel cell contamination. J Power Sources 2009;186(2):435–45.
[30] Fuller T. Electrochemical engineering. Hoboken, NJ, USA: Wiley; 2018.
[31] Hayre R. Fuel cell fundamentals. Hoboken, New Jersey: John Wiley & Sons Inc; 2016.
[32] Amphlett JC, Baumert R, Mann RF, Peppley BA, Roberge PR, Harris TJ. Performance modeling of the ballard mark iv solid polymer electrolyte fuel cell: ii. empirical model development. J Electrochem Soc 1995;142(1):9.
[33] Barbir F. PEM fuel cells : theory and practice. London: Academic Press; 2013.
[34] Höflinger J, Hofmann P, Geringer B. Dynamic multi-parameter sensitive modeling of a pem fuel cell system for bev range extender applications. In: Liebl J, editor. Der Antrieb von morgen 2019. Wiesbaden: Springer Fachmedien Wiesbaden; 2019. p. 171–90.
[35] Falcao D, Gomes P, Oliveira V, Pinho C, Pinto A. 1d and 3d numerical simulations in pem fuel cells. Int J Hydrogen Energy 2011;36(19):12486–98. https://doi.org/10.1016/j.ijhydene.2011.06.133. http://www.sciencedirect.com/science/article/pii/S0360319911016053.
[36] Yuan W, Tang Y, Pan M, Li Z, Tang B. Model prediction of effects of operating parameters on proton exchange membrane fuel cell performance. Renew Energy 2010;35(3):656–66. https://doi.org/10.1016/j.renene.2009.08.017. http://www.sciencedirect.com/science/article/pii/S0960148109003760.
[37] Harms C, Khrmann F, Dyck A. Study of the influence of key test parameters on the performance of a pemfc stack. Solid State Ionics 2015;vol. 275:75–9. https://doi.org/10.1016/j.ssi.2015.03.023. 17th International conference on solid state protonic conductors, Seoul, Korea, 14-19 September 2014, http://www.sciencedirect.com/science/article/pii/S0167273815001058.
[38] Wang S-H, Peng J, Lui W-B, Zhang J-S. Performance of the gold-plated titanium bipolar plates for the light weight pem fuel cells. J Power Sources 2006;162(1):486–91. https://doi.org/10.1016/j.jpowsour.2006.06.084. http://www.sciencedirect.com/science/article/pii/S0378775306012237.
[39] Wang S-H, Peng J, Lui W-B. Surface modification and development of titanium bipolar plates for pem fuel cells. J Power Sources 2006;160(1):485–9. https://doi.org/10.1016/j.jpowsour.2006.01.020. http://www.sciencedirect.com/science/article/pii/S037877530600084X.
[40] S.-H. Wang, W.-B. Lui, J. Peng, J.-S. Zhang, Performance of the iridium oxide (IrO2)-modified titanium bipolar plates for the light weight proton exchange membrane fuel cells, J Fuel Cell Sci Technol 10 (4), 041002. doi:10.1115/1.4024565arXiv:https://asmedigitalcollection.asme.org/electrochemical/article-pdf/10/4/041002/6032056/fc_010_04_041002.pdf. URL https://doi.org/10.1115/1.4024565.
[41] Y. Song, C. Zhang, C.-Y. Ling, M. Han, R.-Y. Yong, D. Sun, J. Chen, Review on current research of materials, fabrication and application for bipolar plate in proton exchange membrane fuel cell, Int J Hydrogen Energy:https://doi.org/10.1016/j.ijhydene.2019.07.231. URL http://www.sciencedirect.com/science/article/pii/S0360319919328745.
[42] Zhang J, Li H. Effect of operating backpressure on pem fuel cell performance. ECS Trans 2009;19:65–76. https://doi.org/10.1149/1.3271363. URL https://doi.org/10.1149/1.3271363.
[43] Zhang J, Wu J, Zhang H. PEM fuel cell testing and diagnosis. 1st ed. London: Newnes; 2013, ISBN 978-0-444-53689-1.
[44] Yan W-M, Wang X-D, Mei S-S, Peng X-F, Guo Y-F, Su A. Effects of operating temperatures on performance and pressure drops for a 256cm2 proton exchange membrane fuel cell: an experimental study. J Power Sources 2008;185(2):1040–8. https://doi.org/10.1016/j.jpowsour.2008.08.053. http://www.sciencedirect.com/science/article/pii/S0378775308016947.
[45] Han I-S, Park S-K, Chung C-B. Modeling and operation optimization of a proton exchange membrane fuel cell system for maximum efficiency. Energy Convers Manag 2016;113:52–65. https://doi.org/10.1016/j.enconman.2016.01.045. http://www.sciencedirect.com/science/article/pii/S0196890416000625.
[46] Chen H, Liu B, Liu R, Weng Q, Zhang T, Pei P. Optimal interval of air stoichiometry under different operating parameters and electrical load conditions of proton exchange membrane fuel cell. Energy Convers Manag 2020;205:112398. https://doi.org/10.1016/j.enconman.2019.112398. http://www.sciencedirect.com/science/article/pii/S0196890419314050.
[47] Sun L, Shen J, Hua Q, Lee KY. Data-driven oxygen excess ratio control for proton exchange membrane fuel cell. Appl Energy 2018;231:866–75. https://doi.org/10.1016/j.apenergy.2018.09.036. http://www.sciencedirect.com/science/article/pii/S0306261918313448.
[48] Chen J, Liu Z, Wang F, Ouyang Q, Su H. Optimal oxygen excess ratio control for pem fuel cells. IEEE Trans Contr Syst Technol 2018;26(5):1711–21.
[49] Chang YA, Moura SJ. Air flow control in fuel cell systems: an extremum seeking approach. In: 2009 American control conference. IEEE; 2009. p. 1052–9.
[50] Amirinejad M, Rowshanzamir S, Eikani MH. Effects of operating parameters on performance of a proton exchange membrane fuel cell. J Power Sources 2006;161(2):872–5. https://doi.org/10.1016/j.jpowsour.2006.04.144. http://www.sciencedirect.com/science/article/pii/S0378775306008093.
[51] Qin Y, Du Q, Fan M, Chang Y, Yin Y. Study on the operating pressure effect on the performance of a proton exchange membrane fuel cell power system. Energy Convers Manag 2017;142:357–65. https://doi.org/10.1016/j.enconman.2017.03.035. http://www.sciencedirect.com/science/article/pii/S0196890417302467.